Rock Mechanics and Rock Engineering
https://doi.org/10.1007/s00603-022-03211-0

ORIGINAL PAPER

On the Effect of Shield Friction in Hard Rock TBM Excavation

Georg H. Erharter[1,2] · Robert Goliasch[3] · Thomas Marcher[1]

Received: 1 July 2022 / Accepted: 21 December 2022
© The Author(s) 2023

Abstract
During hard rock tunnel boring machine (TBM) excavation, shields behind the cutterhead are usually in direct contact with the tunnel wall and therefore subjected to friction forces that occur within this interface. The effect of shield friction in hard rock TBM tunneling has received little attention so far and literature on this topic is scarce and conflicting. To investigate the friction coefficient for the planning of TBM excavations, specialized shear tests were conducted where steel specimens were sheared against lithologically different rock specimens under representative normal forces and shearing speeds. The tests were executed with and without the use of bentonite lubrication. The results show that there is a significant difference between different lithologies and also that using bentonite does not lower the friction coefficient as expected. To elaborate on the effect of shield friction during construction, a framework for interpretation of TBM operational data based on experience from construction sites is provided. Whereas thorough interpretation of the data enables one to draw conclusions about the shield friction, it still remains difficult to assess the real effect of shield friction due to the limited possibilities to observe the ongoing phenomena. This study therefore provides the basis for theoretical and practical assessments of the effect of shield friction for the planning and construction phase of a tunnel. This becomes increasingly important in the light of new contractual developments that aim at differentiating "standard" from "special" advance in an objective and reproducible way.

Highlights

- Thorough elaboration of the effect of shield friction for hard rock tunnel boring machine excavation.
- First presentation of special shear tests to assess the friction coefficient for different rock types, with or without the use of bentonite.
- Discussion of the use of tunnel boring machine operational data to draw conclusions about the effect of shield friction during excavation.
- Questioning the effectiveness of bentonite lubrication for tunnel boring machine excavation.

Keywords TBM tunneling · Hard rock TBM · Shield friction · Shear tests · Bentonite · TBM operational data

Abbreviations

TBM	Tunnel boring machine
TBM-O	Open/gripper TBM
TBM-S	Single shield TBM
TBM-DS	Double shield TBM

1 Introduction

Throughout the past decades, tunnel boring machine (TBM) excavation became the preferred method for tunnels with more than a few kilometers lengths and roughly homogeneous, hard rock conditions. Although TBMs are increasingly used, many aspects of the TBM–rock mass interaction are not fully understood and require further investigation to optimize future planning and operation of TBMs.

✉ Georg H. Erharter
erharter@tugraz.at

[1] Institute for Rock Mechanics and Tunnelling, Graz University of Technology, Rechbauerstraße 12, Graz, Austria

[2] Norwegian Geotechnical Institute (NGI), Sandakerveien 140, Oslo, Norway

[3] Department Tunneling and International, Strabag AG, Donau City Strasse 1, 1220 Vienna, Austria

Published online: 14 January 2023

The effect of shield friction is one of these aspects which is a force that acts against the TBM's thrust (Maidl et al. 2008). More specifically, shield friction can be defined as the static and kinetic frictional resistance that results from the contact between a TBM's shields behind the cutterhead and the surrounding tunnel wall. In the context of this paper, the term shield friction is used for all types of hard rock TBMs (i.e., open-/gripper TBMs: TBM-O, single shield TBMs: TBM-S, double shield TBMs: TBM-DS) even if they only have small shields behind the cutter head (mainly TBM-O). The fact that shield friction acts against the thrust of a TBM is generally known and is mentioned in well-known publications and textbooks (Gehring 1996; Girmscheid 2013; Maidl et al. 2008, 2011, 2013). These works often compute the effect of shield friction (F_f) as a multiplication of the normal force (F_n) that results from the self-weight of a TBM's cutterhead, main drive arrangement and the components behind it, with a friction coefficient (μ) (see, e.g., Girmscheid (2013) p. 452, Eq. 1)

$$F_f \approx F_n * \mu \tag{1}$$

While this physics-based relationship is incontestable, the complex steel–rock interaction in the shield area of a TBM is often not further elaborated and phenomena such as static friction (μ_0) vs. kinetic/sliding friction (μ_k), or different friction coefficients for different types of rocks are not covered. Uncertainties in this regard are also exemplified by conflicting recommendations for friction coefficients between steel and rock (with and without lubrication) for TBMs in literature where, for example, Gehring (1996) recommends to use $\mu_0 = 0.25$–0.45 and $\mu_k = 0.15$–0.3 and Girmscheid (2013) p. 453 recommends $\mu = 0.3$–0.4.

Furthermore, these recommendations are not in accordance with the few direct laboratory investigations of friction between steel and rock. Gaffney (1976) published friction coefficients between steel and different lithologies, but only kinetic friction coefficients at high speeds (> 9.7 m/s) are determined which is not the case in TBM tunneling. The results from Taghipour et al. (2015) are also seen as not representative for TBM applications as they also consider comparably high rotational speeds (> 1.3 m/s) and a "pin on disc" tribometer test set up which is not comparable to the shield–tunnel interaction. Rabbat et al. (1985) published a dry μ_0 of 0.57 and a lubed (water) μ_0 of 0.65 for the contact steel–concrete and a lubed μ_0 of 0.68 for the contact steel–grout but does not elaborate why the lubed coefficients are higher than the dry ones. There are several publications that investigate the interaction between samples and steel plates of rock mechanical testing machinery (Hawkes and Mellor 1970; Rashed and Peng 2015; Xu et al. 2017), but the investigated conditions are not comparable to TBM tunneling and the used lubricants would not be applicable in tunnel applications due to financial and environmental reasons.

Despite the approach to compute F_f based on F_n and μ, some authors report on direct measurements of F_f based on "stroke tests", where a TBM's cutterhead and the front shield are pushed through the tunnel without excavation work. For example Maidl et al. (2008) p. 74, state that a F_f of 12,000–15,000 kN can be expected for a TBM with a diameter of 11–12 m. In contrast to that, Radoncic et al. (2014) determined a F_f of 3500 kN for TBM-DS with a diameter of around 10 m with stroke tests at the Koralm Tunnel and stroke tests at the exploratory tunnel Ahrental-Pfons of the Brenner Base tunnel (Bergmeister and Reinhold 2017; Reinhold et al. 2017) have shown a F_f of around 4000 kN for a TBM-O with a diameter of around 8 m (Erharter and Marcher 2020). While these reports are themselves inconclusive, a deeper investigation of the effect of shield friction is often missing, as the focus is mostly put on the TBM's excavation work. Despite the previously mentioned deficits, closer investigation on the effect of shield friction is even more important as new approaches towards contractual TBM advance classification (Bach et al. 2018; Holzer et al. 2021) are also referring to shield friction as one criterium to discriminate "standard drives" from "special drives".

The goal of the present study is to approach the problem of estimating F_f from several sides. It is emphasized that this study considers the topic of shield friction in non-squeezing, hard rock conditions (for squeezing conditions, see, e.g., Hasanpour et al. (2014); Hasanpour et al. (2015); Hasanpour et al. (2018); Mohammadzamani et al. (2019); Ramoni and Anagnostou (2010, 2011); Zhang and Zhou (2017)). First, theoretical considerations on the interaction between a TBM's shield and the surrounding rock mass are presented (Sect. 2), followed by results from laboratory experiments in Sect. 3, where μ was experimentally determined. Direct shear tests with and without bentonite lubrication were conducted between different rock types and hardened TBM-shield steel plates. In Sect. 4, approaches to estimate F_f from TBM operational data are shown and Sect. 5 and 6 aim at discussing the results and bring together theoretical considerations, experimental results, and analyses based on TBM operational data.

2 Theoretical Aspects on Shield–Rock Interaction

2.1 General Aspects

To excavate rock mass, a TBM exerts an advance force (F_a) via the cutterhead onto the tunnel face. F_a is, however, only

a part of the total thrust (F_t) in advance direction, as resistive forces (F_r) act against it (Eq. 2)

$$F_a = F_t - F_r \tag{2}$$

The shield friction (F_f) is therefore a part of F_r and comes from the direct contact between a TBM's shield and the tunnel wall. Besides that, F_r consists mainly of resistances within the machinery and mechanics of the TBM itself (F_m, i.e., internal mechanical friction and the dragging force of the backup system) and the so-called "subcritical penetration" (F_{sp}). Frenzel et al. (2012) and Wilfing et al. (2016) describe F_{sp} as the range of advance force where the cutterhead is in contact with the face, but the applied force is not sufficiently high to initiate the chipping process. They further describe that F_{sp} consists of two parts, where first the thrust is so low that not even crushing of the rock directly under the cutters is induced (herein termed as F_{sp1}) and at higher levels of thrust the rock below the cutters is crushed, but chipping does not yet occur (herein termed F_{sp2}). F_{sp1} is considered to be a part of F_r as it is within the range of thrust where excavation is not yet possible (i.e., penetration = 0). F_{sp2} is considered to be the lower range of F_a where the penetration slowly starts to increase due to a sufficient amount of thrust. Consequently F_f can be computed directly by subtracting F_m, F_{sp} and F_a from F_t (Eq. 3)

$$F_f = F_t - F_m - F_{sp1} - F_a \tag{3}$$

In this study, only tunnel excavations that are "sub-horizontal" are considered, since in case of an inclined excavation, the effect of gravity on the machine must be considered as well. A summary of all used symbols is given in Table 3 in the Appendix and an overview of the mentioned components of the thrust in Fig. 1.

Theoretically, F_f can be furthermore subdivided into a static friction force (F_f^0) and a kinetic friction force (F_f^k) depending on whether μ_0 or μ_k is used to compute it where usually $F_f^0 > F_f^k$ (e.g., Demtröder (2017) p. 217), and based on Eq. 1, it follows:

$$F_f^0 \approx F_n * \mu_0 \tag{4}$$

$$F_f^k \approx F_n * \mu_k \tag{5}$$

Finally, some basic laws of friction (Amontons 1699; Coulomb 1821, 1973; Popova and Popov 2015) need to be mentioned as they will be discussed later:

- The friction is directly proportional to the normal load.
- Kinetic frictional resistance does not depend on the respective velocity.

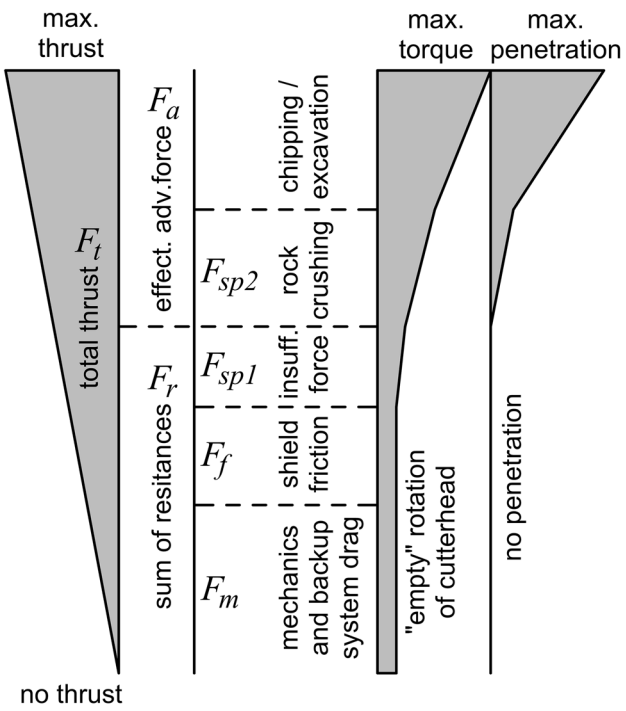

Fig. 1 Overview of the main forces that act on the total thrust of a TBM. The cutterhead torque and the penetration rate are also displayed for later reference. All shown relationship between forces are purely qualitative

- Friction is independent of the contact area.

2.2 TBM Type-Specific Shield–Rock Interaction

Further examination of friction force F_f requires an insight into the mechanical achievements of state-of-the-art hard rock TBMs. As initially described, open gripper TBMs (TBM-O) as well as shielded TBMs (TBM-S, TBM-DS) are designed for advance in hard rock conditions. All these machine types are excavating full face, with no active face support and in atmospheric environment.

The normal load reacting on the invert of the shield as well as the shield contact area are different between these types as well as the shield functions. Additionally, the open gripper TBMs can be divided into single gripper TBMs with long main beam and into multi-gripper TBMs, known as Kelly TBM. Considering the dead weight of these machines in a single span beam model, the normal load on the front shield can be calculated in a static analysis, although it varies with depending on the extension of a stroke. Table 1 and Fig. 2 give an overview of the different TBM types and how they are affected by the effect of shield friction.

Table 1 Overview of hard rock TBM types and their shield–friction interaction

Hard rock TBMs	Extraction method of shield structure	Shield–friction interaction
Gripper TBM type main beam (TBM-O; Fig. 2a)	Massive invert shield segment to support the main drive and cutterhead, hydraulically extendable side and roof shield, landed to the wall during advance for cutterhead stabilization	Appr. 2/3 TBM load on invert shield, additional friction due to hydraulic extended side and roof support possible
Gripper TBM type Kelly (TBM-O; Fig. 2b)	Geometrical small invert and roof shield due to main drive at rear section and guidance of cutter head with long gripper frame, hydraulic extendable invert and roof shield to compensate cutter wear	Appr. 1/2 TBM load on invert shield, additional friction due to hydraulic extended roof support possible. Load on the front shield changes with extended stroke length
Single shield TBM (TBM-S; Fig. 2c)	Massive front shield to support the main drive und cutterhead, middle shield graded to front shield with optional articulation, tail shield graded to middle shield	Full TBM load on invert shied, due to shield gap theoretically no further contact areas on sides and roof
Double shield TBM (TBM-DS; Fig. 2d)	Massive front shield to support the main drive und cutterhead, outer telescopic shield graded to front shield, gripper and tailshield graded. Outer and inner telescopic shield sliding against each other during TBM advance	Full TBM load on invert front and outer telescopic shield, due to shield gap theoretically no further contact areas on sides and roof. Friction between outer and inner telescopic shield possible due to steering movements, gripper and telescopic shield not effected in DS mode

2.3 Contact Geometry and Influencing Factors

Shielded TBMs within a tunnel can be thought of like a small cylinder within a large one, and thus, theoretically, there is only a contact line with an infinitely small contact area (Fig. 3) which is also true if the shield is built with a certain conicity (i.e., slightly tapered towards the end). In practice, however, it can be assumed that the lower half-, to lower third of a TBM's shield is always in contact with the tunnel wall and crushed material within the "shield gap" (i.e., the gap between the shield and the tunnel wall, Fig. 3).

Depending on the type of TBM, possibilities to visually observe the shield gap are limited, and therefore, the actual contact area cannot be determined exactly. In the case of TBM-S or TBM-DS, the shield gap can only either be observed from the existing "geologists' windows" within the shield (i.e., 2–4, roughly 0.5×0.5 m-sized windows in different positions behind the main drive of the TBM, Fig. 5), by looking against the advance direction from openings in the upper cutterhead or by looking in advance direction from openings in the first precast concrete segments behind the shield (normally used for backfilling).

Several effects influence (raising or lowering) the frictional contact between a TBM's shield and the tunnel wall and are connected to the overall TBM geometry, the way the TBM is operated, and the surrounding rock mass conditions (Fig. 6):

- TBM-S/TBM-DS are usually built with shields that are tapered via a conical shield and/or steps within it. The tapered shape helps to prevent blocks and other material getting stuck in the shield gap (see prev. section) as well as to reduce the influence of minor water ingress.
- Steering operations affect the effect of shield friction as TBMs are sometimes driven in a "slanting" way which provokes stress concentrations on edges and/or jamming of the whole shield within the tunnel.
- Vibrations from the excavation process are likely also influencing the effect of shield friction, although further investigations are required to determine if it increases or decreases it.
- A major influence is seen in the rock mass conditions. On the one hand, stress controlled rock mass behavior can lead to similar problems like squeezing rock mass (Ramoni and Anagnostou 2010, 2011), where the TBMs shield might become fully stuck due to plastic rock mass deformation. On the other hand, discontinuity driven and blocky (Delisio et al. 2013; Delisio and Zhao 2014) rock mass behavior can lead to blocks of different sizes being jammed in between the shield and the tunnel wall (examples are given in Figs. 4 and 5a and b).
- In several excavations, it can be observed that the TBM's shield is "swimming" in a bed of silty to gravelly debris

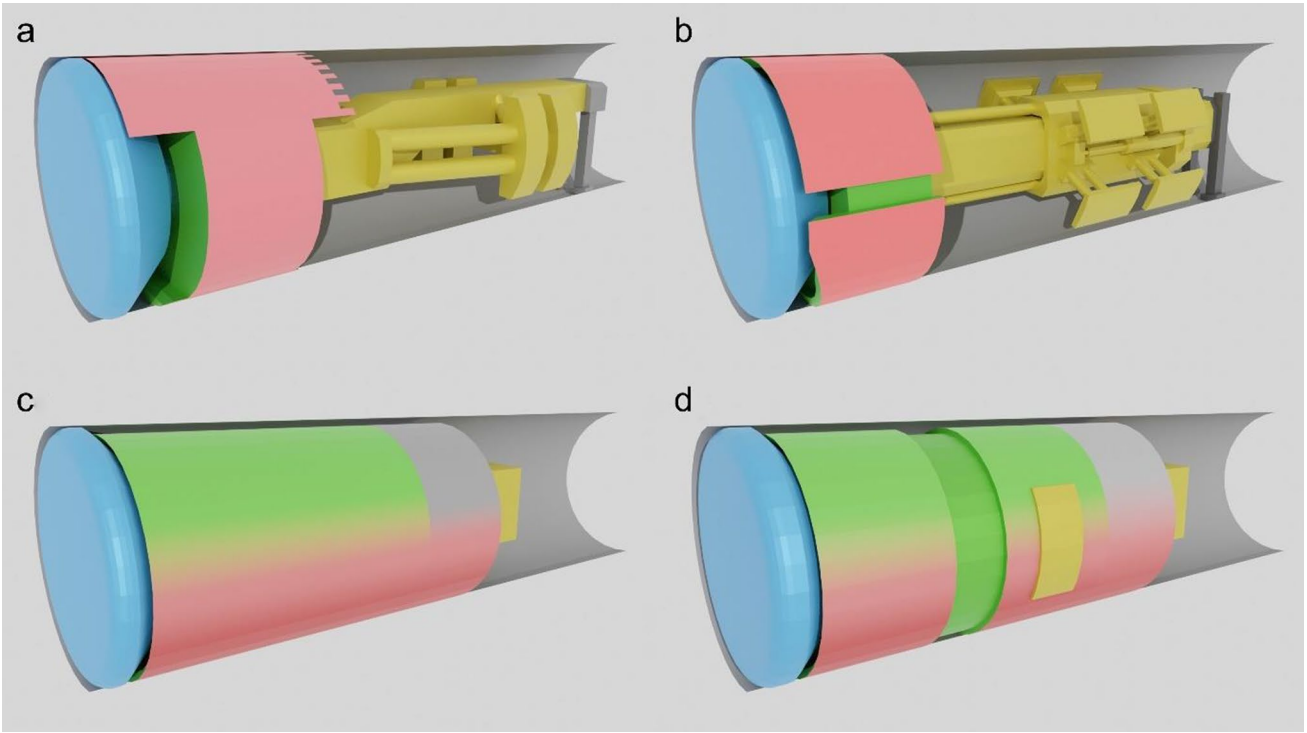

Fig. 2 Visualization of different hard rock TBM types (colors: blue: cutterhead, yellow: backup system and gripper, and red/green: shield area) and how they are affected by the effect of shield friction; **a** gripper TBM type main beam, **b** gripper TBM type Kelly, **c** single shield TBM, and **d** double shield TBM

that is deposited within the shield gap (i.e., crushed and grinded material that results from the excavation process, Fig. 5c). Due to the rotation direction of the cutterhead, there is usually an accumulation of this material on one side of the machine, thus leading to an asymmetric geometry of this bed and an asymmetric contribution to the effect of shield friction (visualized in Fig. 6).

- Theoretically, the overcut should not directly affect the shield friction as the contact line between shield and tunnel stays the same, irrespective of the diameter difference. On the one hand, during the excavation, a bigger overcut creates a bigger gap between the shield and the tunnel wall and thus allows for bigger accumulations of crushed material in the shield gap. It also decreases the arching effect of the tunnel itself and thus provokes bigger overbreaks (Girmscheid 2013). On the other hand, a bigger overcut reduces the danger of getting stuck due to squeezing rock mass conditions.

3 Laboratory Determination of Friction Coefficients

To determine μ_0 and μ_k for different rock types and with or without lubrication, a series of direct shearing tests was conducted. μ_0 can be computed from the ratio of the shear strength immediately after the start of the shear test τ_{start} (corresponding to F_f^0 in section 2.1) to the normal stress σ_n (corresponding to F_n in section 2.1.; see also Eq. 4) and

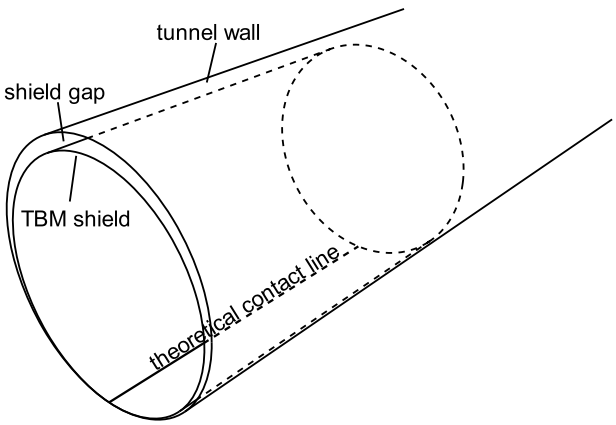

Fig. 3 Theoretical geometry of a TBM within a tunnel

Fig. 4 Stitched panoramic view from a video recording out of an opening in precast concrete segments from behind a TBM-DS's shield. View direction is into advance direction. An overbreak caused up to m-sized blocks to be lying on the shield

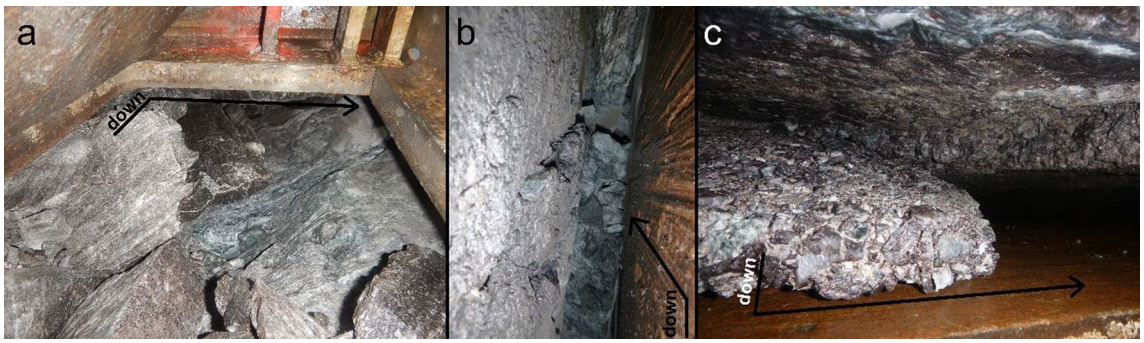

Fig. 5 Different views through "geologists' windows" in a TBM-DS onto the surrounding rock mass. Arrows indicate the advance direction and the vertical orientation of the image. **a** Looking upwards, a fully jammed shield gap that is filled with dm-sized blocks. **b** Looking in advance direction, the shield gap is fully jammed with crushed material of different sizes. Also note the up to cm—deep scratches in the shield resulting from jammed blocks during advance. **c** Looking downwards, the lower part of the TBM is "swimming" in a bed of crushed material that fills the shield gap

μ_k from the ratio of the remaining shear strength τ_{res} (corresponding to F_f^k in section 2.1; see also Eq. 5) after the start to σ_n. As given in section 2.1 for many material combinations, one could expect that τ_{start} is greater than τ_{res} as once the initial static friction is overcome, the kinetic friction should be lower. An idealized / "to be expected" result of a shear test is shown in Fig. 7.

3.1 Test Setup

To conduct shear tests for determining the effect of shield friction, both steel and rock specimen were produced. The steel specimen has a "Hardox 450" hardened steel plate (dimensions 15 × 15 × 0.8 cm) as well as a S355 high-quality construction steel at its base which is welded onto a standard construction steel plate S335 with dimensions 13 × 13 × 2 cm (Fig. 8). Hardened "Hardox 450" steel is

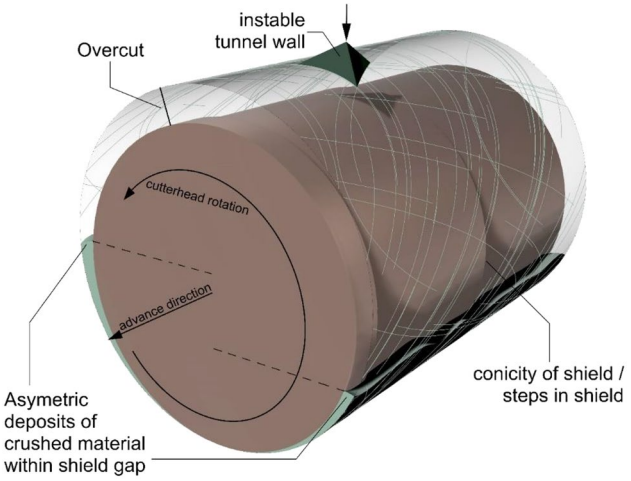

Fig. 6 Influences on the effect of shield friction with the example of a single shield TBM (note: disproportionally small TBM for visualization purposes)

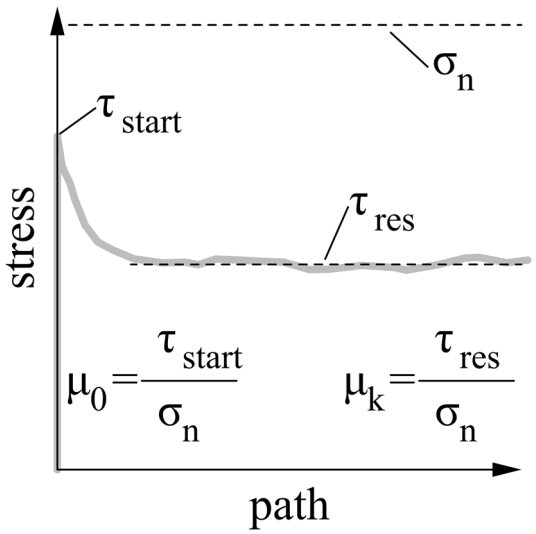

Fig. 7 Idealized/to be expected shear test to determine static (μ_0) and kinetic (μ_k) friction coefficients of a material

used to reinforce construction elements that are subjected to increased wear, such as the lower part of hard rock TBM shields. S355 high-quality construction steel is mainly getting used for standard shield structures. The hardened steel plate is welded onto a thicker standard steel plate to increase the contact area to the cement that is used to fix the specimen within one of the shear test's shearing boxes. To further strengthen the "steel-specimen to cement to shear box" connection, three steel rods with screw threads were welded onto the mounting plate. Screw nuts were attached to the rods' ends to positions the steel specimen in a perfectly level position within the shearing box. Figure 8 shows a drawing of the steel specimen, the final steel specimen, and the steel specimen cemented into a shearing box.

The rock specimens were cut to dimensions of 15 × 15 × 8–10 cm, so that they can be properly cemented into the shearing boxes. The used bentonite for the lubricated shearing tests is the same product as it is used to lubricate hard rock TBM excavations. 40 g of bentonite were mixed into 1 l of water and the suspension was given at least 12 h time to rest before application, so that the clay minerals had sufficient time for swelling (recipe based on construction site experience).

3.2 Testing Program

Based on the assumption that the rock surface properties of a tunnel wall are changing as the TBM shield moves over it, every shear test was repeated ten times (called "cycles"). For every cycle, the upper shear box was lifted and set back to the original position without contact to the rock sample, so that the shearing direction was kept constant. The shearing path for one cycle was 50 mm. To investigate friction coefficients for different rock types, samples from four different lithologies were used (Table 2).

The surface of the rock specimen was not specially treated and can be described as "rough cut" with a standard rock saw but still would be characterized as "planar" and "smooth" according to ÖNORM EN ISO 14689, 2019. The applied shearing speed was determined based on TBM operational data (see Sect. 3.2.1) and the vertical force was determined following a simple static model (see Sect. 3.2.2). In addition to these, process-oriented methods of determining a realistic shearing speed and vertical load, some exploratory tests with limestone samples were conducted in advance to the main test series. As part of the exploratory tests, the vertical force was varied between 5 and 50 kN and the shearing speed between 10 and 100 mm/min but no significant influence of these parameters on the friction coefficient was observed (thus confirming basic friction laws for the selected test conditions as given in the end of Sect. 2.2). A discussion on the influence of shearing speed and vertical load on the friction coefficient is given in Sect. 5. In total, 13 shearing test series (i.e., 13 × 10 single shearing tests/cycles) were conducted. The shearing test machinery during a test is shown in Fig. 9.

3.2.1 Determination of Shearing Speed

The used shearing speed for the tests was based on the advance speeds of two TBM projects which were available for analysis to the authors. While a median advance speed of 51.5 mm/min was achieved at the exploratory tunnel Ahrental-Pfons of the Brenner Base Tunnel in Austria (Bergmeister and Reinhold 2017; Reinhold et al. 2017), a median of 31.6 mm/min was achieved at the Ulriken tunnel

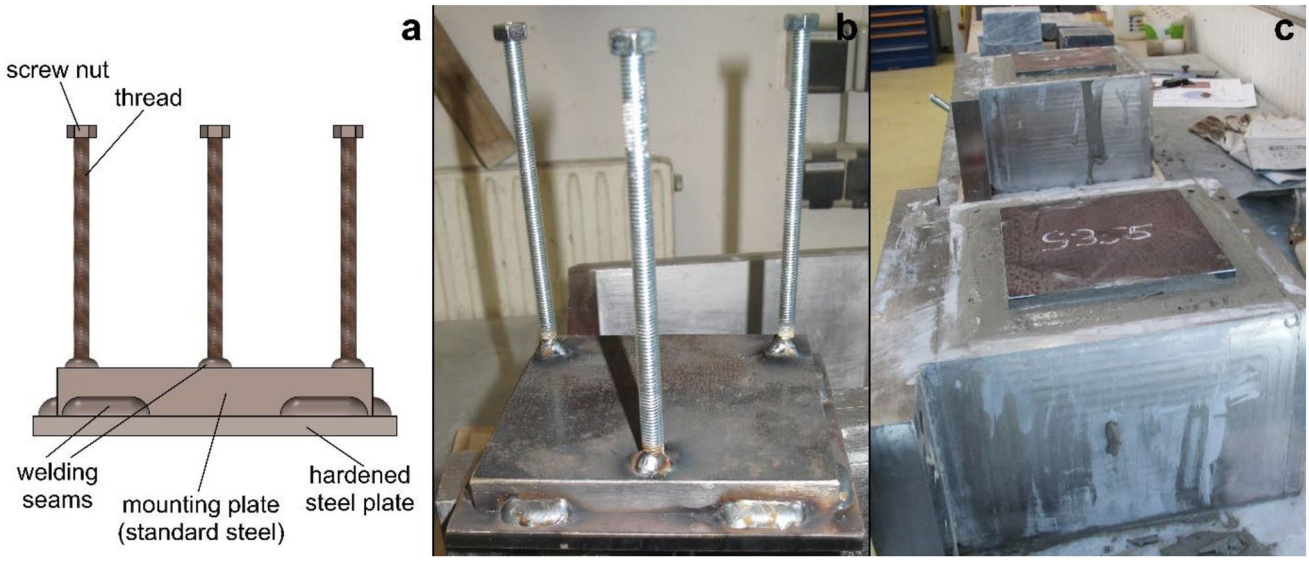

Fig. 8 **a** Plan of the steel specimen. **b** Image of the final steel specimen. **c** A steel specimen that is cemented into the shearing box and ready for testing

Table 2 Overview of the used lithologies to produce rock specimen for shear testing

Lithology	Formation	Sample origin	References
Limestone	Kanzelkalk (Graz Paleozoic)	Quarry "Kanzelsteinbruch Gratkorn GmbH"	e.g., (Flügel 2000)
Basalt	Pliocene intrusion, Styrian Basin	Quarry "ALAS Klöch GmbH"	e.g., (Gross et al. 2007; Schnepp et al. 2021)
Granite	Brixner Granite	Brenner Base Tunnel—BBT SE, South Tyrol	e.g., (Brandner et al. 2008; Sander 1906)
Quartz phyllite	Innsbrucker Quartzphyllite	Brenner Base Tunnel—BBT SE, North Tyrol	e.g., (Brandner et al. 2008; Haditsch and Mostler 1982)

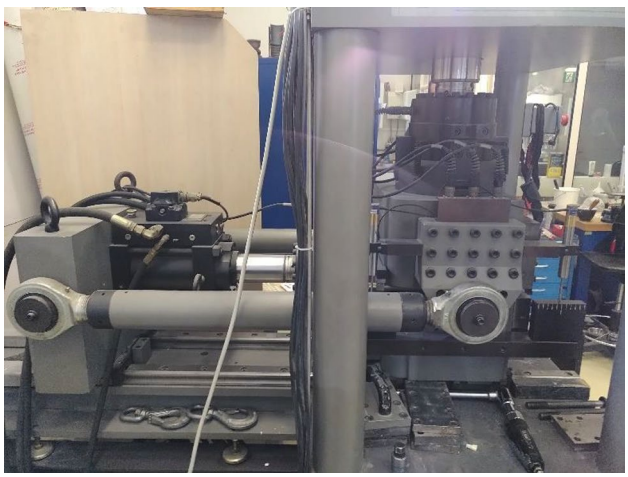

Fig. 9 Direct shearing test machine that was used to conduct the tests to determine friction coefficients

in Norway (Macias et al. 2017; Rekve 2017). Although both excavations were done using similar open gripper TBMs, the different advance rates can be related to the rock mass conditions which were rather soft, metamorphic rocks for the exploratory tunnel Ahrental-Pfons and mostly hard rock, igneous lithologies for the Ulriken tunnel.

As a TBM's stroke usually starts with a slower speed which is then increased to the desired advance speed, two shearing speeds within the total 50 mm shearing path of one single test were applied: a shearing speed of 10 mm/min was used for the first 5 mm of the tests and then a shearing speed of 40 mm/min for remaining 45 mm which is based on the above-given observations.

3.2.2 Determination of Vertical Load

With the supplier's weight specifications of three hard rock TBMs, TBM-O main beam and Kelly, as well as TBM-S in a diameter range of about 5 m, the operating weight effective on the shield was assessed. This value was referred to the in the field experienced friction areas of TBM types as stated in Sect. 2.2. The friction area includes 180 rad for TBM-Os due to hydraulic extendable shield arrangements and 90 rad for TBM-S/DS due to rock fines filling up the shield from

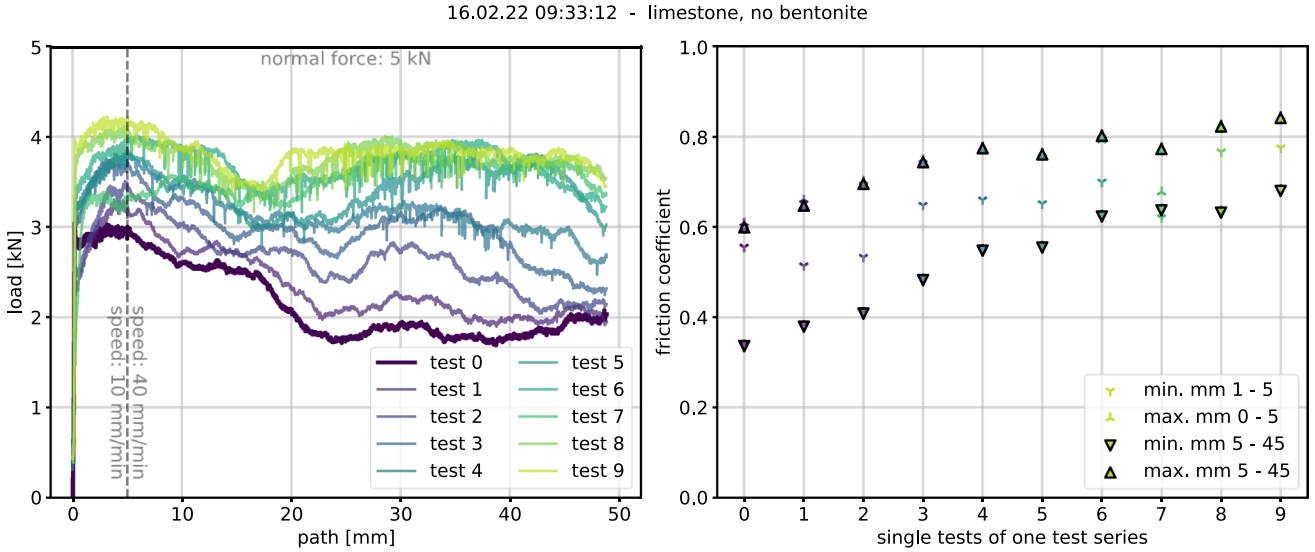

Fig. 10 Recording of a shear test series with limestone and no bentonite lubrication. The left diagram shows the recorded horizontal load over the course of 50 mm test paths of the ten single shear tests in the series. The right diagram shows min.–max. values for all single tests of the series, separated into values for the path between 0 and 5, 1 and 5, and 5 and 45 mm. A general increase of the friction coefficient from one test to the next is observable

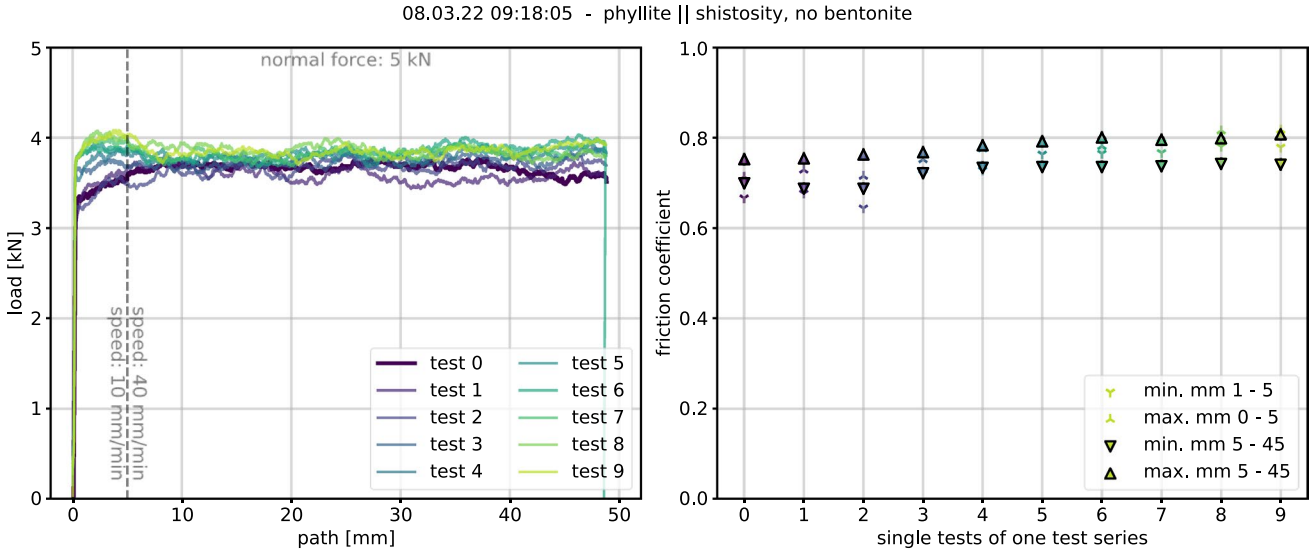

Fig. 11 Recording of a shear test series with phyllite and without bentonite lubrication where the shearing direction is parallel to the schistosity. No increase of the friction coefficient from one test to the next and a generally low variability is observable (see Fig. 10 for a description of the diagrams)

invert center line ± 45 deg. as an experienced assumption. The applied scenarios led to results between 200 and 250 kN/m^2 vertical load for the different machine types. Applied on the 15 × 15 cm steel test plate (i.e., 225 cm^2), 5 kN of normal force were used for the shear testing program of this study.

3.3 Results

The tests confirmed that friction coefficients vary between combinations of steel with different lithologies. Visualizations as well as the raw test data of all individual tests are given in the Supplementary information of the paper. The following general observations were made:

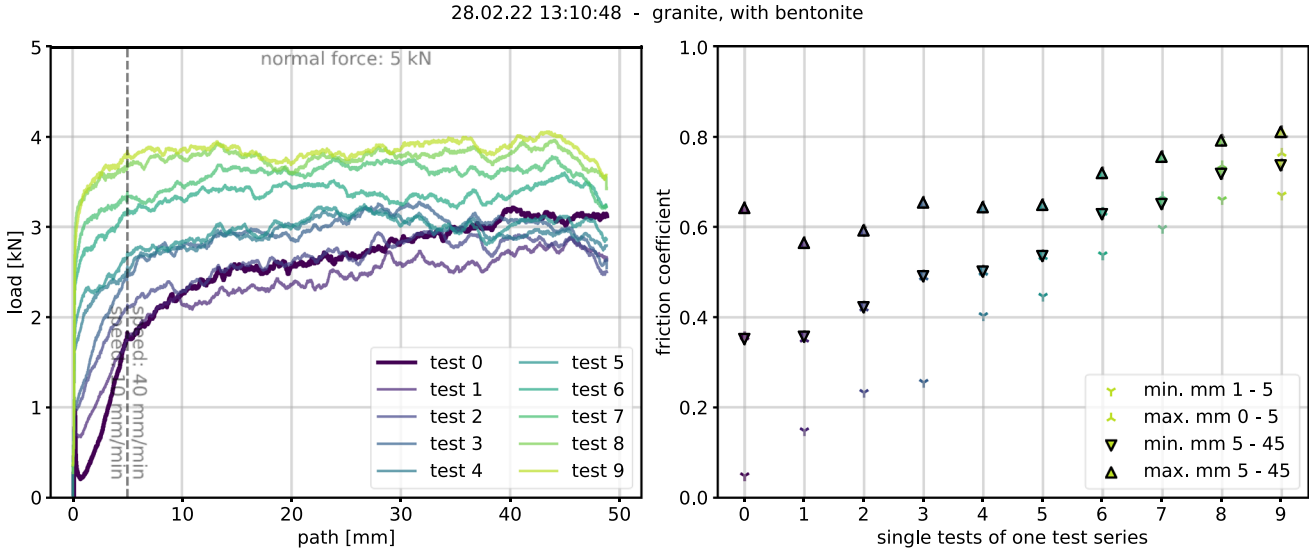

Fig. 12 Recording of a shear test series with granite and bentonite lubrication. A pronounced increase of the friction coefficient from one test to the next is observable (see Fig. 10 for a description of the diagrams)

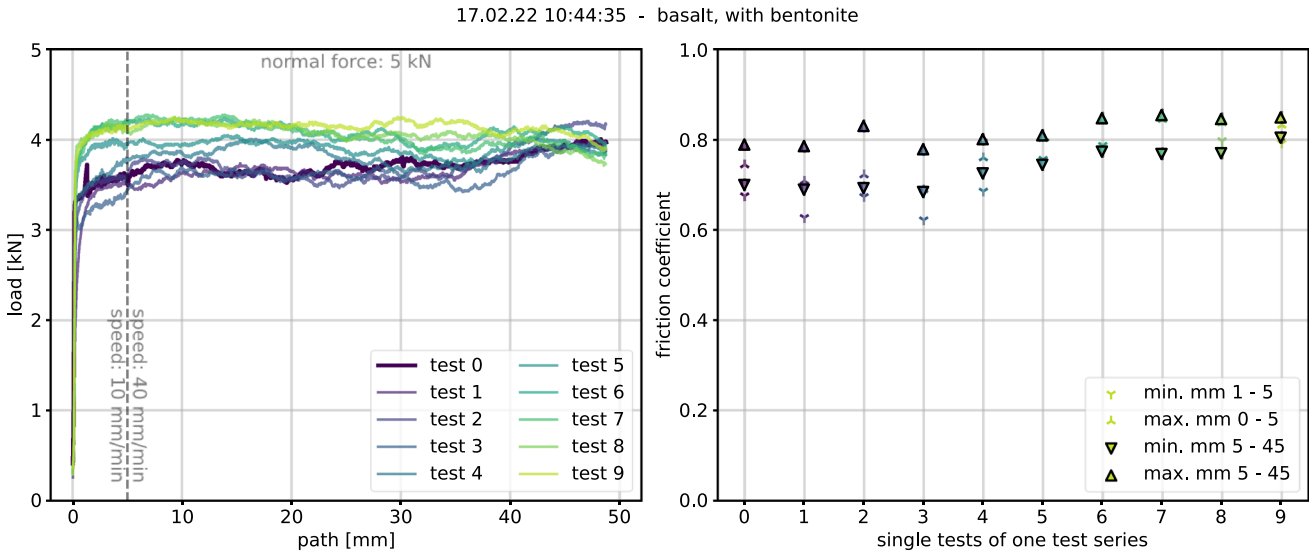

Fig. 13 Recording of a shear test series with basalt and bentonite lubrication. No clear effect of the bentonite is observable (see Fig. 10 for a description of the diagrams)

1. High variability within one single test path (i.e., a min–max range of μ of up to 0.35) can be observed for some lithologies (Fig. 10) but not for all (Fig. 11).
2. High variability within one test series (i.e., 10 cycles) can be observed, where an increase of μ from the first to the last test occurs. This varies between lithologies but is pronounced in tests with bentonite lubrication (Figs. 10, 12).
3. The majority of tests show no clear "static friction peaks" (see beginning of section 3 and Fig. 7) at the beginning of a test (Figs. 10, 11, 12, 13).
4. Bentonite mainly affects the μ_k of the first few tests within one test series and there is a pronounced difference between lithologies with respect to how strong the effect is (Figs. 12, 13).
5. Highest variability within one test series usually can be observed within the first few tests of that series and many test series show less variability within the last 3–4 single tests of them (Figs. 10, 11, 12, 13).

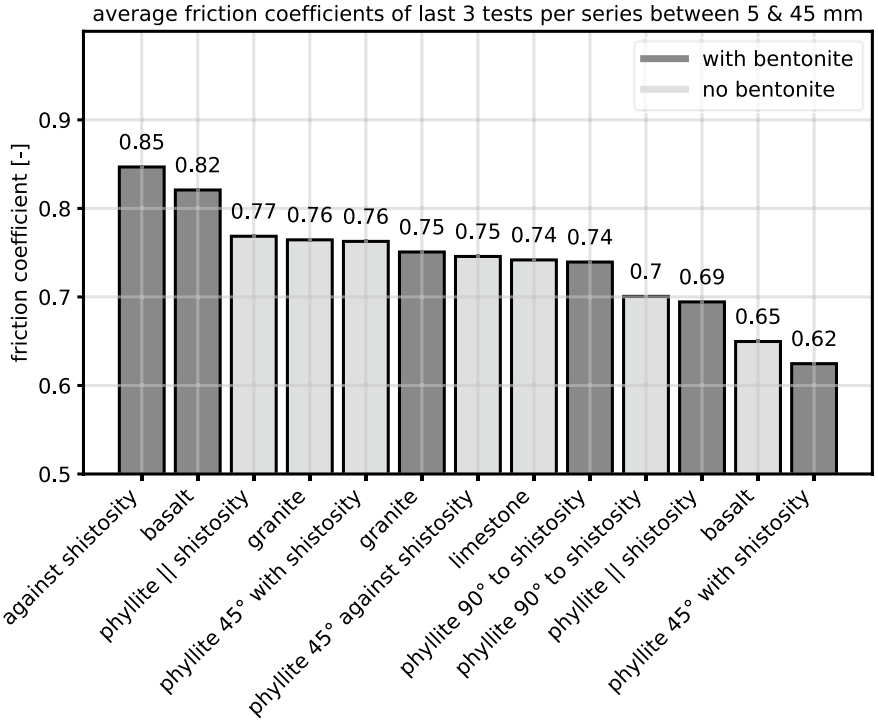

Fig. 14 Graphical representation of the results where the friction coefficient for each lithology was computed as the average value of the test paths between 5 and 45 mm of the last three single tests of one test series. Whereas there is a difference of friction coefficients between lithologies, no pronounced effect of the usage of bentonite can be observed

Due to these observations and as the goal of the tests was to derive friction coefficients that are usable in practice, the further analysis was done as follows: the single tests were divided into a startup phase from mm 0–5 (i.e., with a shearing speed of 10 mm/min) and a main phase between mm 5–45 (i.e., with a shearing speed of 40 mm/min). The last 5 mm were not considered, due to the increased occurrence of outliers. Due to the observation that the variability within one test series decreases towards the end of a series, an arithmetic mean of the main phases of the last three tests of one test series was used to get the final friction coefficient. The results of this analysis are presented in Fig. 14 and the corresponding tabular data can be found in file "All_results.xlsx" in the Supplementary information.

This result analysis leads to the observation that friction coefficients differ between lithologies. The application of bentonite has a highly variable influence on the material's frictional characteristics. A general decrease of the friction coefficient due to the application of bentonite cannot be observed, and in several cases, the tests with bentonite even show significantly higher friction coefficients than without. A significant decrease in friction coefficient due to the application of bentonite can only be observed for the tests of phyllite with the shearing direction parallel to the schistosity and the phyllite sample that was sheared 45° in the direction of the schistosity. A deeper discussion of this analysis is given in section 5.

4 Shield Friction Estimation Based on TBM Operational Data

Whereas the previous section considered determination of the friction coefficient with laboratory data, another approach to estimate the effect of shield friction is to derive it from the TBM operational data. In Eq. 3 (see Sect. 2.1), it is shown how the shield friction can be computed if all the required forces are known and can be gathered from the TBM's data records. For cases where there is insufficient knowledge about these forces, the TBM data need to be interpreted manually, and usually, the total advance force, the cutterhead's torque, and the penetration rate are used for this. Although "experience based TBM data interpretation" is common practice on construction sites, there are very few publications on it in general and especially not about TBM data-based shield friction estimations.

Recently, the "theoretical advance force" ($F_{a\text{theo}}$) was presented by Heikal et al. (2021) which allows one to compute F_r directly (therein termed the "advance force loss"). Based on Eq. 2, Eq. 6 can be formulated to estimate F_r and this value can be used as a reference point in TBM data interpretation

$$F_r = F_t - F_{a\text{theo}} \tag{6}$$

This approach shall be shown with an exemplary stroke from the Ulriken tunnel (see section 3.2.1 for references

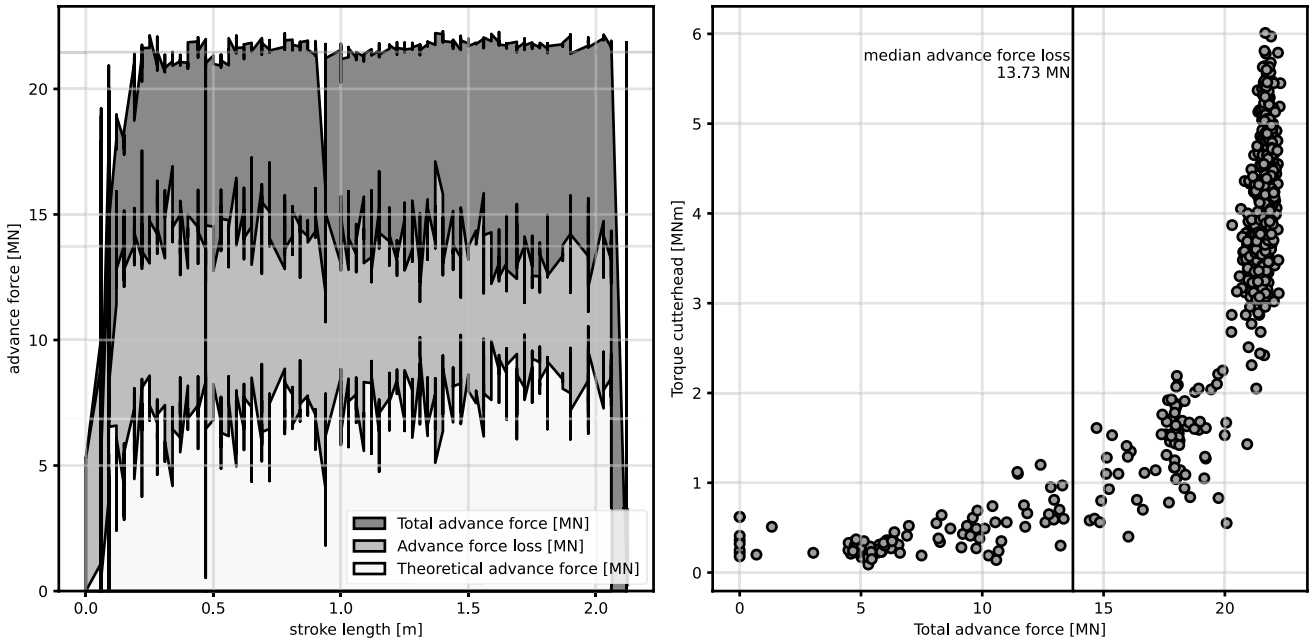

Fig. 15 TBM operational data from an exemplary stroke of the Ulriken tunnel. Left: measured total advance force, computed theoretical advance force, and advance force loss over the length of the stroke. Right: scatterplot of the total advance force vs. the cutterhead torque of the same stroke

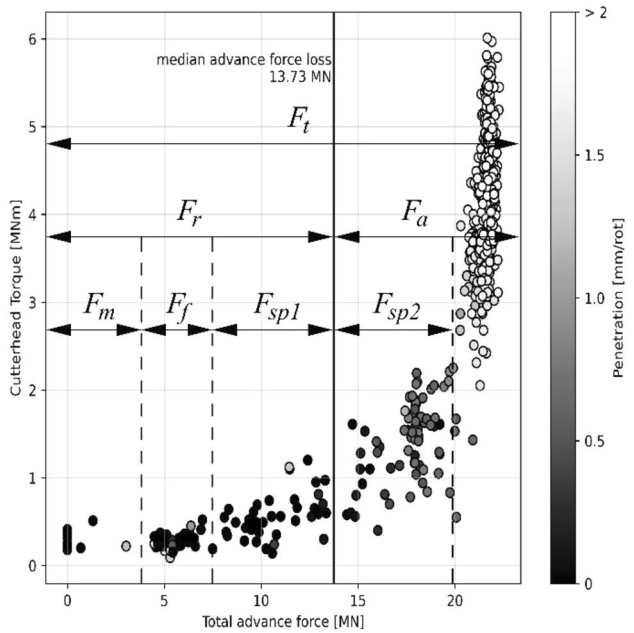

Fig. 16 An interpreted advance force vs. cutterhead torque diagram with color coding according to the penetration rate, based on Fig. 15. See Sect. 2.1 for an explanation of the symbols. The dashed lines indicate that these boundaries were manually interpreted

on the Ulriken tunnel project). In Fig. 15 left, it can be seen that (in this case) $F_{a\text{theo}}$ is approximately a third of the max. total advance force and the rest is lost due to different phenomena (see Sect. 2.1). In Fig. 15 right, a scatterplot of total advance force vs. cutterhead torque is shown as well as the median F_r (i.e., advance force loss) of the whole stroke.

Going deeper with this visual analysis, further conclusions about F_r and the forces of which it consists—namely F_m, F_f, and F_{sp1} (see Sect. 2.1)—can be drawn from the TBM operational data if no further information is available. In Fig. 16, a more complex visualization of Fig. 15 (right) is given and interpreted boundaries for these forces are shown.

The boundaries in Fig. 16 are based on these considerations (also shown in Fig. 1):

- The sequence with which F_m, F_f, and F_{sp} come into effect should be the same for most strokes as the TBM first has to overcome internal resistances (F_m), then the shield friction (F_f) when the cutterhead moves towards the face and finally the subcritical penetration (F_{sp}, consisting of F_{sp1} and F_{sp2}; see Sect. 2.1) occurs when the cutterhead is in contact with the face, but the force is not yet sufficiently high to initiate the chipping process.
- A lower boundary of F_f resp. upper boundary of F_m was in this case estimated by interpreting multiple strokes and repeatedly observing a pronounced cluster at around 5 MN. Up to the upper boundary of F_f, the penetration can be >0 in some datapoints, since the machine is moving towards the face.

- An upper boundary of F_f can be estimated by looking for the range of data where the advance force increases, but there is no pronounced increase of the cutterhead torque beyond the torque that is required to rotate the cutterhead on its own, since the cutterhead is not yet in contact with the face.
- The range of F_{sp} is characterized by a simultaneous increase of both advance force and cutterhead torque. While in the range of F_{sp1}, the penetration is almost completely 0, since no rock crushing is yet going on, in the range of F_{sp2}, the penetration rate is slowly increasing towards the final penetration that is necessary to initiate the chipping process. The boundary between F_{sp1} and F_{sp2} (i.e., upper boundary of F_r) can be estimated by these criteria, or also via computation of the "advance force loss" acc. Heikal et al. (2021) which correlates well with it.
- Since F_{sp2} is not considered to be a part of F_r as the penetration rate is already > 0 mm/rot it shall not be further discussed herein, but in depth explanations on the mechanism of the subcritical penetration can be found in Frenzel et al. (2012) and Wilfing et al. (2016).

It has to be noted that the presented interpretation of the exemplary stroke of Figs. 15 and 16 cannot be done with every stroke due to the inherent variability that is present in TBM operational data. In practice, analysis of many strokes, practical experience from the construction site, consultation of the TBM operators as well as comparison of the TBM data to the encountered geological conditions is required to facilitate meaningful interpretations.

5 Discussion

In Sect. 3.3, results of μ for each lithology were shown by taking the average of the last three cycles of each test series. Besides the therein given justification that most test series tend to converge towards a final value within its last cycles, the last values are additionally seen as more representative for the steel–rock friction that is dominant for the largest part of the TBM shield. The idea is, that the low values of μ which occur within the first few cycles of one series are in reality only likely to occur in the front area of the shield, where it is in contact with the freshly cut surface of the tunnel wall. The longer the shield moves over one point of the tunnel wall, the more the μ at the contact point approaches the values which was measured towards the end of one test series. Further studies are, however, necessary to estimate within which distance this increase of μ occurs from the front to the back of a TBM's shield.

In contrast to Gehring (1996) or Girmscheid (2013) who recommend values of μ between 0.15 and 0.45 for the interaction of steel and (unspecified) rock (see the introduction), the herein presented laboratory results show higher values for μ for all investigated rock types with a range between 0.62 and 0.85. In reality, it is likely that these high μ values would be slightly damped, as the TBM's shield is not only in contact with the tunnel wall's rock but also with crushed material within the lower part of the shield gap (see Sect. 2, Figs. 5c and 6). In the authors' experience, this crushed material can usually be characterized as a slightly silty, sandy gravel (si', sa, Gr acc. to EN ISO 14688-1 (2019)), and for example, Herzog (1985) recommends values of μ between 0.2 for the contact of steel to silty- and 0.55 for steel to gravelly soils (see also Ambrosi (2019)). Nevertheless, in practice, it is not possible to determine exactly to what extent the TBM's shield is in direct contact with the tunnel wall's rock and with the crushed material in the shield gap. It is therefore recommended that the final μ for planning purposes is computed as an average of lithology-specific laboratory values as presented in Sect. 3.3 and 0.55 acc. to Herzog (1985) (e.g., for an excavation in granite without the application of bentonite: $(0.76 + 0.55) * 0.5$ gives a $\mu \approx 0.65$).

Comparing the herein determined values of μ between steel and rock to those of other authors (see the introduction) shows for example a good accordance with the results for steel–concrete of Rabbat et al. (1985) who also used a comparable test setup. The results differ, however, substantially from those of, e.g., Gaffney (1976) or Taghipour et al. (2015). The reason for that is seen in the fact that these studies investigated steel–rock friction under much higher speeds where effects such as vaporization of volatile components of the rock (i.e., water vapor production or thermal breakdown of $CaCO_3$) come into play and are therefore not representative for TBM tunneling.

Beyond the determined, lithology-specific values for μ, no evidence for a distinction between static and kinetic friction coefficients for any steel–rock system was observed. Almost no "static friction peaks" at the start of the individual experiments were observed and it seems like the dynamic friction is higher than the static one. An explanation for this could be that the ongoing shearing process creates finely, crushed material in the steel–rock interface which might show a dilative behavior, but further investigations on this are needed.

Although injection of bentonite into the shield gap is often the "go-to" approach in situations, where there is concern that a TBM might get stuck, no evidence was found that bentonite has a beneficial effect in the sense that it lowers the friction coefficient between steel and rock. In some tests with bentonite, lower friction coefficients were observed in the first few tests (e.g., Fig. 12) which can be explained with the fact that the bentonite was smeared onto the rock surfaces before the test, and consequently, a large part of it was pressed out as the tests went on. It can be concluded that bentonite could

lower the friction between steel and rock if one was able to effectively get it into that interface. This means that bentonite lubrication is likely only effective when it is applied as a preventive measure before a TBM is fully stuck. Once there are too many existing contact points between rock and a TBM's shield, it is unlikely that bentonite can be pressed in between, and therefore, the bentonite's effectiveness to lower the effect of shield friction in these situations is highly questionable.

With respect to the investigated anisotropic samples of the Innsbrucker Quartzphyllite, no significant connection between μ and the angle of test execution to the schistosity could be observed for unlubricated tests. The lubricated tests with anisotropic rocks had the biggest spread in μ and marked the maximum and minimum values of all test series with μ s of 0.85 and 0.62, respectively. It was observed that the μ for a shearing direction 45° with schistosity < parallel to schistosity < 90° to schistosity < 45° against schistosity (see Fig. 14). It consequently seems like the effectiveness of bentonite is related to the anisotropy of this lithology. In practice, however, this observation might be hard to be put to use, since detailed knowledge of the rock's anisotropy is often not available due to limited possibilities of observing the rock mass (see Sect. 2.3).

Knowing the μ between shield and rock is valuable for theoretical estimations of F_f. New contractual developments for TBM tunneling (e.g., current revision of ÖNORM B 2203-2, 2005 as presented in Bach et al. (2018); Holzer et al. (2021)) call for deeper estimations of shield friction. Visual interpretation of TBM operational data as presented in section 4 might be a well-suited supplement to theoretical considerations involving μ. If one can estimate the normal force of the TBM due to its self-weight based on the TBM's technical documentation, the full-scale μ (i.e., including contacts between shield–rock and shield–crushed material in shield gap) could be back calculated.

It has to be stated that the approach of TBM data interpretation presented in section 4 is highly interpretative and experience dependent. The therein discussed upper limit of F_r which is partly based on Heikal et al. (2021) is, however, in good accordance with the work about "subcritical penetration" of Frenzel et al. (2012) and Wilfing et al. (2016). The upper limits of F_f are also in good accordance with the construction site reports of the shield friction given in Frenzel et al. (2012); Radoncic et al. (2014) or Erharter and Marcher (2020). In contrast to that, the proposed values for F_f of 12,000–15,000 kN from Maidl et al. (2008) do neither fit to the presented approach in section 4 nor to the mentioned reports of shield friction from construction sites. The range of 12,000–15,000 kN does, however, fit to the presented upper limit of F_r and the upper limit of the subcritical penetration from Frenzel et al. (2012) and Wilfing et al. (2016), thus giving rise to the assumption that Maidl et al. (2008) is actually referring to the upper limit of all resistive forces (F_r) and not only the effect of shield friction alone.

6 Conclusion and Outlook

This study contributed to better understanding the interaction between hard rock TBMs' shields and the surrounding tunnel wall. For the first time, specialized laboratory shear tests were conducted to investigate the steel–rock interaction for shearing speeds and normal force conditions that are representative for TBM tunneling and friction coefficients were estimated for different lithologies. Furthermore, estimations of shield friction based on TBM operational data were made, as a supplementary method to theoretical considerations based on the laboratory determined friction coefficients.

Nevertheless, this study is seen as one of the first steps towards fully understanding the frictional contact between hard rock TBMs and the rock mass. One future contribution would be to extend on this study by performing more shear tests between steel and different lithologies to extend the catalogue of friction coefficients. Another aspect that could be worth to investigate is the effect of surface roughness on the friction coefficients, since the herein presented tests have been performed with sawed rock surfaces (see Sect. 3.2). While smooth surfaces improve repeatability of results, the actual tunnel surface is usually rougher with potential consequences for the friction coefficient.

On a bigger scale, further investigations are required to better estimate how much of a TBM's shield is in direct contact with the rock and how much is in contact with the crushed material that fills up the lower part of the shield gap. It furthermore needs to be emphasized that the present study mostly addresses TBM tunneling under stable rock mass conditions, and it can be assumed that different effects come into play when the tunnel face is instable and the TBM's thrust cannot be properly transferred into rock mass anymore and thus an increase of F_n can be expected. As in many other geotechnical investigations, scale effects might also play an important role for the steel–rock interaction which can be of significance, since the herein determined friction coefficients are based on 15 × 15 cm large intact rock samples. Discontinuities in a fractured rock mass can lead to a different friction coefficient for the system steel–rock mass than in the system steel–rock and also introduce a certain "rock mass anisotropy" that differs from the lithological anisotropy that results from layering and schistosity. Finally, it was found that the effectiveness of bentonite as a support measure to help reduce the effect of shield friction of a TBM is questionable and alternative measures should be investigated that better deal with already existing steel–rock contacts.

Table 3 List of used symbols

Symbol	Description
μ	General friction coefficient with no specification of static or kinetic friction
μ_0	Static friction coefficient
μ_k	Kinetic friction coefficient
F_t	Total thrust of a TBM
F_a	Effective advance force that acts on the rock face via the cutter head
F_{atheo}	Theoretical advance force after Heikal et al. (2021)
F_r	Sum of all resistive forces that at against the total thrust of a TBM
F_f	General shield friction force (part of F_r)
F_m	Force that results from internal mechanical processes and dragging of the backup system of a TBM (part of F_r)
F_{sp}	Advance force of the "subcritical penetration" that is exerted against the tunnel face before the chipping process begins
F_{sp1}	Part of F_{sp} before crushing of rock beneath the cutters is initiated and where the penetration is mostly = 0
F_{sp2}	Part of F_{sp} after crushing of the rock beneath the cutters is initiated, but before chipping has started. Penetration slowly increases
F_n	Normal force of the front part of the TBM due to its self-weight
F_f^0	Static friction force
F_f^k	Kinetic friction force

Supplementary Information The online version contains supplementary material available at https://doi.org/10.1007/s00603-022-03211-0.

Acknowledgements The BBT SE is highly acknowledged for providing samples from the Innsbrucker Quartzphyllite and the Brixner Granit and the TBM operational data from the exploratory Ahrental Pfons. BaneNor is thanked for providing the TBM operational data from the Ulriken Data for further analysis. The Kanzelsteinbruch Gratkorn GmbH and the ALAS Klöch GmbH are thanked for providing limestone and basalt samples from their quarries. Strabag–BMTI workshop in Spittal/Drau is thanked for providing the parts to build the steel specimen for the experimental part of this study. The input and discussions about the thrust vs. torque plots with Mr. Helmut Wannenmacher were also very valuable for the study. Support by geo.zt—poscher beratende geologen zt-gmbh is also highly acknowledged. Finally, Prof. Manfred Blümel and Mr. Anton Kaufman of the rock mechanics laboratory of the Institute of Rock Mechanics and Tunnelling are thanked for their efforts of executing the large amount of shear tests that was required.

Author Contributions Conceptualization: GHE, RG, and TM. Data curation: GHE. Formal analysis: GHE and RG. Funding acquisition: TM. Investigation: GHE, RG, and TM. Methodology: GHE, RG, and TM. Project administration: GHE. Resources: TM and RG. Software: GHE. Supervision: TM. Visualization: GHE. Writing—original draft: GHE and RG. Writing—review and editing: TM.

Funding Open access funding provided by Graz University of Technology.

Data availability The used TBM operational data cannot be shared due to confidentiality. The collected laboratory data can be found in the "Supplementary Information" of the paper.

Open Access This article is licensed under a Creative Commons Attribution 4.0 International License, which permits use, sharing, adaptation, distribution and reproduction in any medium or format, as long as you give appropriate credit to the original author(s) and the source, provide a link to the Creative Commons licence, and indicate if changes were made. The images or other third party material in this article are included in the article's Creative Commons licence, unless indicated otherwise in a credit line to the material. If material is not included in the article's Creative Commons licence and your intended use is not permitted by statutory regulation or exceeds the permitted use, you will need to obtain permission directly from the copyright holder. To view a copy of this licence, visit http://creativecommons.org/licenses/by/4.0/.

References

Ambrosi M (2019) Appraisal of frictin coefficients between TBM and conditioned soil: a laboratory investigation adopting a direct shear apparatus. Master's Thesis, Delft University of Technology

Amontons G (1699) De la resistance cause'e dans les machines (about resistance and force in machines). Mem l'Acedemie, pp 257–282

Bach D, Holzer W, Leitner W, Radončić N (2018) The use of TBM process data as a normative basis of the contractual advance classification for TBM advances in hard rock. Geomechanik Und Tunnelbau 11:505–518. https://doi.org/10.1002/geot.201800042

Bergmeister K, Reinhold C (2017) Learning and optimization from the exploratory tunnel—Brenner Base Tunnel. Geomechanik Und Tunnelbau 10:467–476. https://doi.org/10.1002/geot.201700039

Brandner R, Reiter F, Töchterle A (2008) Überblick zu den ergebnissen der geologischen vorerkundung für den Brenner-Basistunnel. Geo Alp, pp 165–174

Coulomb CA (1821) Theorie des machines simple (Theory of simple machines). Bachelier

Coulomb CA (1973) Essai sur une application des regles de maximis et minimis a quelques problemes de statique relatifs a l'architecture (Essay on maximums and minimums of rules to some static problems relating to architecture). In: Memoires de Mathematique & de Physique, presentes a I' Academie. Royale des Sciences par divers Savans, & Ius dans ses Assemblees, 7th edn, pp 343–382

Delisio A, Zhao J (2014) A new model for TBM performance prediction in blocky rock conditions. Tunn Undergr Space Technol 43:440–452. https://doi.org/10.1016/j.tust.2014.06.004

Delisio A, Zhao J, Einstein HH (2013) Analysis and prediction of TBM performance in blocky rock conditions at the Lötschberg Base Tunnel. Tunn Undergr Space Technol 33:131–142. https://doi.org/10.1016/j.tust.2012.06.015

Demtröder W (2017) Mechanics and thermodynamics. Springer International Publishing, Cham

EN ISO 14688-1 (2019) Geotechnische Erkundung und Untersuchung—Benennung, Beschreibung und Klassifizierung von Boden. Österreichisches Normungsinstitut

Erharter GH, Marcher T (2020) MSAC: Towards data driven system behavior classification for TBM tunneling. Tunn Undergr Space Technol 103:103466. https://doi.org/10.1016/j.tust.2020.103466

Flügel HW (2000) Die lithostratigraphische gliederung des paläozoikums von Graz (Österreich). In: Flügel HW, Hubmann B (eds) Das paläozoikum von Graz: stratigraphie und bibliographie. Verl. der Österr. Akad. der Wiss, Wien, pp 7–59

Frenzel C, Galler R, Käsling H, Villeneuve M (2012) Penetration tests for TBMs and their practical application/penetrationstests für tunnelbohrmaschinen und deren anwendung in der Praxis. Geomechanik Tunnelbau 5:557–566. https://doi.org/10.1002/geot.201200042

Gaffney ES (1976) Measurements of dynamic friction between rock and steel

Gehring KH (1996) Design criteria for TBM's with respect to real rock pressure. In: Wagner H, Schulter A (eds) Tunnel boring machines. CRC Press, pp 43–53

Girmscheid G (2013) Bauprozesse und bauverfahren des tunnelbaus, 3rd edn. Ernst & Sohn, Berlin

Gross M, Fritz I, Piller WE, Soliman A, Harzhauser M, Hubmann B, Moser B, Scholger R, Suttner TJ, Bojar H-P (2007) The Neogene of the Styrian Basin—guide to excursions: das neogen des steirischen beckens—exkursionsführer. Johannea Geol Paläont 9:117–193

Haditsch JG, Mostler H (1982) Zeitliche und stoffliche gliederung der erzvorkommen im Innsbrucker quarzphyllit. Geologische Paläontologische Mitteilungen Innsbruck, pp 1–40

Hasanpour R, Rostami J, Ünver B (2014) 3D finite difference model for simulation of double shield TBM tunneling in squeezing grounds. Tunn Undergr Space Technol 40:109–126. https://doi.org/10.1016/j.tust.2013.09.012

Hasanpour R, Rostami J, Barla G (2015) Impact of advance rate on entrapment risk of a double-shielded TBM in squeezing ground. Rock Mech Rock Eng 48:1115–1130. https://doi.org/10.1007/s00603-014-0645-2

Hasanpour R, Rostami J, Thewes M, Schmitt J (2018) Parametric study of the impacts of various geological and machine parameters on thrust force requirements for operating a single shield TBM in squeezing ground. Tunn Undergr Space Technol 73:252–260. https://doi.org/10.1016/j.tust.2017.12.027

Hawkes I, Mellor M (1970) Uniaxial testing in rock mechanics laboratories. Eng Geol 4:179–285. https://doi.org/10.1016/0013-7952(70)90034-7

Heikal G, Erharter GH, Marcher T (2021) A new parameter for TBM data analysis based on the experience of the Brenner Base Tunnel excavation. IOP Conf Ser: Earth Environ Sci 833:12158. https://doi.org/10.1088/1755-1315/833/1/012158

Herzog M (1985) Die Pressenkräfte bei Schildvortrieb und Rohrvorpressung im Lockergestein. BMT Baumaschine + Bautechnik 32:236–238

Holzer W, Wagner OK, Leitner W (2021) Überarbeitung der österreichischen Werkvertragsnorm ÖNorm B 2203–2 für den kontinuierlichen Vortrieb. Geomechan Tunn 14:730–739. https://doi.org/10.1002/geot.202100057

Macias FJ, Andersson T, Eide L (2017) Project control by using the NTNU model methodology: the new Ulriken Tunnel. In: Proceedings of the World Tunnel Congress 2017: Surface challenges—underground solutions

Maidl B, Schmid L, Ritz W, Herrenknecht M (2008) Hardrock tunnel boring machines. Ernst, Berlin

Maidl B, Herrenknecht M, Maidl U, Wehrmeyer G (2011) Maschineller tunnelbau im schildvortrieb, 2nd edn. Ernst, Berlin

Maidl B, Thewes M, Maidl U, Sturge D (2013) Handbook of tunnel engineering, 1st edn. Ernst/Wiley, Berlin

Mohammadzamani D, Mahdevari S, Bagherpour R (2019) Evaluation of required thrust force based on advance rates in shielded TBMs under squeezing conditions. J Geophys Eng 16:842–861. https://doi.org/10.1093/jge/gxz050

ÖNORM B 2203–2 (2005) Untertagebauarbeiten—werkvertragsnorm. Österreichisches Normungsinstitut, Wien

ÖNORM EN ISO 14689 (2019) Geotechnische erkundung und untersuchung—benennung, beschreibung und klassifizierung von fels. Österreichisches Normungsinstitut

Popova E, Popov VL (2015) The research works of Coulomb and Amontons and generalized laws of friction. Friction 3:183–190. https://doi.org/10.1007/s40544-015-0074-6

Rabbat BG, ASCE M, Russell HG (1985) Friction coefficient of steel on concrete or grout. J Struct Eng 111:505–515

Radoncic N, Hein M, Moritz B (2014) Determination of the system behaviour based on data analysis of a hard rock shield TBM/Analyse der Maschinenparameter zur Erfassung des Systemverhaltens beim Hartgesteins-Schildvortrieb. Geomechanik Und Tunnelbau 7:565–576. https://doi.org/10.1002/geot.201400052

Ramoni M, Anagnostou G (2010) Tunnel boring machines under squeezing conditions. Tunn Undergr Space Technol 25:139–157. https://doi.org/10.1016/j.tust.2009.10.003

Ramoni M, Anagnostou G (2011) The interaction between shield, ground and tunnel support in TBM tunnelling through squeezing ground. Rock Mech Rock Eng 44:37–61. https://doi.org/10.1007/s00603-010-0103-8

Rashed G, Peng SS (2015) Change of the mode of failure by interface friction and width-to-height ratio of coal specimens. J Rock Mech Geotechn Eng 7:256–265. https://doi.org/10.1016/j.jrmge.2015.03.009

Reinhold C, Schwarz C, Bergmeister K (2017) Development of holistic prognosis models using exploration techniques and seismic prediction. Geomechanik Und Tunnelbau 10:767–778. https://doi.org/10.1002/geot.201700058

Rekve M (2017) Numerisk stabilitetsvurdering av bergstabbe i Ulriken tunnel ved TBM driving. In: Dunham KD, Dammyr Ø, Rømoen M, Engen S (eds) Fjellsprengningsdagen, Bergmekanikkdagen, Geoteknikkdagen

Sander B (1906) Geologische beschreibung des brixner Granits. Jahrbuch d k k Geol. Reichsanstalt, p 707

Schnepp E, Arneitz P, Ganerød M, Scholger R, Fritz I, Egli R, Leonhardt R (2021) Intermediate field directions recorded in Pliocene basalts in Styria (Austria): evidence for cryptochron C2r.2r-1. Earth Planets Space 73:182. https://doi.org/10.1186/s40623-021-01518-w

Taghipour A, Ytrehus JD, Lund B, Skalle P, Lund M, Prakash B (2015) Friction and wear characteristics of steel on rock under water and oil based lubricated sliding conditions. Tribol Mater Surf Interfaces 9:85–91. https://doi.org/10.1179/1751584X15Y.0000000004

Wilfing L, Käsling H, Goliasch R, Moritz B, Thuro K (2016) Penetration tests at the Koralm Tunnel (KAT2) - The right tool to improve penetration prediction in TBM tunneling?/Penetrationsversuche am Beispiel des Koralmtunnels (KAT2)—Ein Werkzeug zur Verbesserung von Penetrationsprognosen im maschinellen Tunnel. Geomechanik Tunnelbau 9:200–209. https://doi.org/10.1002/geot.201600005

Xu YH, Cai M, Zhang XW, Feng XT (2017) Influence of end effect on rock strength in true triaxial compression test. Can Geotech J 54:862–880. https://doi.org/10.1139/cgj-2016-0393

Zhang J-Z, Zhou X-P (2017) Time-dependent jamming mechanism for single-shield TBM tunneling in squeezing rock. Tunn Undergr Space Technol 69:209–222. https://doi.org/10.1016/j.tust.2017.06.020

Publisher's Note Springer Nature remains neutral with regard to jurisdictional claims in published maps and institutional affiliations.